

Rip3 knockdown rescues photoreceptor cell death in blind *pde6c* zebrafish

IA Viringipurampeer¹, X Shan¹, K Gregory-Evans¹, JP Zhang¹, Z Mohammadi¹ and CY Gregory-Evans^{*1}

Achromatopsia is a progressive autosomal recessive retinal disease characterized by early loss of cone photoreceptors and later rod photoreceptor loss. In most cases, mutations have been identified in *CNGA3*, *CNGB3*, *GNAT2*, *PDE6C* or *PDE6H* genes. Owing to this genetic heterogeneity, mutation-independent therapeutic schemes aimed at preventing cone cell death are very attractive treatment strategies. In *pde6c*^{w59} mutant zebrafish, cone photoreceptors expressed high levels of receptor-interacting protein kinase 1 (RIP1) and receptor-interacting protein kinase 3 (RIP3) kinases, key regulators of necroptotic cell death. In contrast, rod photoreceptor cells were alternatively immunopositive for caspase-3 indicating activation of caspase-dependent apoptosis in these cells. Morpholino gene knockdown of *rip3* in *pde6c*^{w59} embryos rescued the dying cone photoreceptors by inhibiting the formation of reactive oxygen species and by inhibiting second-order neuron remodelling in the inner retina. In *rip3* morphant larvae, visual function was restored in the cones by upregulation of the rod phosphodiesterase genes (*pde6a* and *pde6b*), compensating for the lack of cone *pde6c* suggesting that cones are able to adapt to their local environment. Furthermore, we demonstrated through pharmacological inhibition of RIP1 and RIP3 activity that cone cell death was also delayed. Collectively, these results demonstrate that the underlying mechanism of cone cell death in the *pde6c*^{w59} mutant retina is through necroptosis, whereas rod photoreceptor bystander death occurs through a caspase-dependent mechanism. This suggests that targeting the RIP kinase signalling pathway could be an effective therapeutic intervention in retinal degeneration patients. As bystander cell death is an important feature of many retinal diseases, combinatorial approaches targeting different cell death pathways may evolve as an important general principle in treatment.

Cell Death and Differentiation (2014) 21, 665–675; doi:10.1038/cdd.2013.191; published online 10 January 2014

Photoreceptor cell death is a common phenotypic end point associated with inherited retinal degenerations.¹ Although in many cases the causative genetic defects are known, the underlying mechanisms by which photoreceptor degeneration and cell death occurs is not fully understood. Previous studies have identified caspase-dependent apoptosis as a critical factor in retinal diseases,^{1,2} however, more recently caspase-independent mechanisms of apoptosis have been proposed.³ For example, DNA damage leading to excessive activation of DNA repair enzymes such as poly-ADP-ribose polymerase (Parp) causes an increase in oxidative stress, mitochondrial damage and subsequent apoptotic cell death in the *rd1*, P23H and S334ter rodent models of retinal degeneration.^{4,5} Similarly, activation of the calcium-dependent cysteine protease calpain can result in an increase in reactive oxygen species (ROS), mitochondrial damage and lysosomal membrane disruption leading to apoptotic cell death in the retina.⁵

Recently, the necroptosis mechanism of cell death^{6,7} has been implicated in other types of retinal defects such as retinal detachment,⁸ retinal ischemia⁹ and ocular coloboma.¹⁰ In these cases, either cell death was delayed by the inhibitor necrostatin-1, which targets receptor interacting protein kinase 1 (RIP1)¹¹ or the presence of elevated receptor interacting protein kinase 3 (RIP3) was detected, suggesting that cell death in the retina maybe dependent on these key regulators of necroptosis.^{12,13}

Congenital achromatopsia (ACHM) is a progressive autosomal recessive cone disorder¹⁴ characterized by photophobia, nystagmus, poor visual acuity, eccentric fixation and severe deficits in color discrimination.¹⁵ Complete and incomplete forms of ACHM have been described relating to the severity of the disease. Mutations in five genes (*CNGA3*, *CNGB3*, *GNAT2*, *PDE6C*, *PDE6H*) that encode proteins of the phototransduction pathway have been implicated in the

¹Department of Ophthalmology and Visual Sciences, University of British Columbia, Vancouver, BC V5Z 3N9, Canada

*Corresponding author: CY Gregory-Evans, Department of Ophthalmology and Visual Sciences, University of British Columbia, 2550 Willow Street, Vancouver, BC V5Z 3N9, Canada. Tel: +1 604 875 5529; Fax: +1 604 875 4663; E-mail: cge30@mail.ubc.ca

Keywords: RIP3; RIP1; *Pde6c*; retina; zebrafish; achromatopsia

Abbreviations: cGMP, cyclic guanosine monophosphate; *CNGA3*, cyclic nucleotide gated channel α 3; *CNGB3*, cyclic nucleotide gated channel β 3; Daxx, death-domain-associated protein 6; EGFP, enhanced green fluorescent protein; GAPDH, glyceraldehyde-3-phosphate dehydrogenase; GluR2, glutamate receptor subunit 2; *GNAT2*, guanine nucleotide binding protein, alpha transducing 2; H&E, hematoxylin and eosin; Nrl, neural retina-specific leucine zipper; PBS, phosphate-buffered saline; *Pde6c*, cone-specific cGMP phosphodiesterase α -subunit; *PDE6H*, cone-specific cGMP phosphodiesterase γ -subunit; PGAM5, phosphoglycerate mutase family member 5; *Rip1*, receptor-interacting protein kinase 1; *Rip3*, receptor-interacting protein kinase 3; RT-PCR, reverse transcriptase-PCR; STAT3, signal transducer and activator of transcription 3; T α CP, α subunit of cone transducin; Tg, transgenic; TNF α , tumor necrosis factor α ; TUNEL, terminal deoxynucleotidyl transferase dUTP nick end labeling; zpr1, zebrafish double-cone photoreceptor antibody; Parp, poly-ADP-ribose polymerase; d.p.f., days post fertilization; h.p.f., hours post fertilization; FACS, fluorescent-activated cell sorting; PKG, protein kinase G; VBA, visual background adaptation; SIRT2, sirtuin 2

Received 03.9.13; revised 15.11.13; accepted 22.11.13; Edited by N Bazan; published online 10.1.14

pathogenesis of ACHM and result in clinically indistinguishable forms of the disease.^{16–18} However, the cause of ACHM in 10–20% patients remains unresolved, implying further heterogeneity. A zebrafish model of human achromatopsia (*pde6c*^{w59}) has been recently identified displaying rapid degeneration of cone photoreceptors caused by a mutation in the cone phosphodiesterase α -subunit gene (*pde6c*).¹⁹ In this blind mutant, cone outer segments appear to form normally by 3 days post fertilization (d.p.f.), after which there is a rapid loss of cone cells. In addition, genetically normal rod photoreceptors degenerate in the vicinity of the dying cones in the central retina, a so-called bystander effect.²⁰ This bystander cell death effect is seen in human retinal disease²¹ and mouse models of retinal degeneration,²² and represents a critical challenge to overcome in designing gene replacement strategies for retinal degeneration.

To further evaluate the *pde6c*^{w59} mutant as a model for retinal degeneration, and in particular to get a better understanding of the mechanistic framework driving cell death in the different photoreceptor cell types, we investigated caspase-dependent and -independent pathways and their contribution to pathogenesis.

Results

***Pde6c*^{w59} – / – retinal phenotype.** A stable transgenic (Tg) zebrafish line *Tg(T α CP:EGFP)* expressing enhanced green fluorescent protein (EGFP) in cones cells via a cone transducin promoter fragment²³ was crossed to heterozygous carriers of the *pde6c*^{w59} mutation to obtain heterozygous *Tg(T α CP:EGFP)-pde6c*^{w59} carrier zebrafish. As it not possible to visually distinguish between homozygous and heterozygous *Tg(T α CP:EGFP)-pde6c*^{w59} embryos during early development, a simple PCR protocol for genotype analysis from fin DNA was used (Figure 1a). Up to 3 d.p.f., the development of the *Tg(T α CP:EGFP)-pde6c*^{w59} mutant retina is equivalent to wild-type/heterozygous eyes; however, from days 4 to 7 there is a decline in the number of Tg GFP-expressing cone photoreceptors (Figure 1b) and condensed cone nuclei are clearly visible by histology (Figure 1c). There is a single layer of rods remaining in the central area of degenerating cones, whereas the newly formed photoreceptors at the peripheral margins are preserved (Figure 1c). In the central retina, some of the rods nuclei are condensed and rounded-up, suggesting that there is an adverse effect on the genotypically normal rod photoreceptors (Figure 1d).

Cell death in the retina. As there is rapid cone degeneration in the *pde6c*^{w59} mutant retina, we examined larvae from 3 to 7 d.p.f. using terminal deoxynucleotidyl transferase dUTP nick end labeling (TUNEL) staining as a marker for cell death on the non-Tg background. At 3 d.p.f., very few TUNEL-positive cells were detected either in whole-mount wild-type or mutant eyes (Figures 2a and b) or in sections through the retina (Figures 2c and d). At 4 d.p.f. during the height of cone degeneration, many TUNEL-positive cells were observed in whole-mount mutant eyes compared with wild-type (Figures 2e and f) and this was also seen in sections through the retina (Figures 2g and h). At 7 d.p.f., there were still TUNEL-positive cells present in the mutant

whole-mount eyes compared with wild type (Figures 2i and j) and in corresponding retinal sections (Figures 2k and l).

Although we observed a high level of TUNEL-positive cells corresponding to the time at which there is most cone degeneration at 4 d.p.f., this does not inform on the underlying mechanism of cell death. We initially confirmed the molecular and biochemical abnormalities in this model and then examined markers of caspase-dependent and caspase-independent cell death. In the *pde6c*^{w59} mutant retina at 3.5 d.p.f., there were still some double cones present detected by zebrafish double-cone photoreceptor antibody (zpr1) immunohistochemistry (Figure 3a), but they were not immunoreactive for *pde6c* (compare Figures 3a and b) confirming the underlying genetic defect. Based on other phosphodiesterase mutants, mutation of the *pde6c* gene would be predicted to lead an accumulation of cyclic guanosine monophosphate (cGMP).²⁴ We observed a dramatic accumulation of cGMP in the *pde6c*^{w59} mutant retina at 4 d.p.f., demonstrating the biochemical consequence of *pde6c* gene mutation (compare Figures 3c and d) and also the absence of zpr1 cone photoreceptor staining in the mutant (Figure 3c). If cone cell death was mediated through a caspase-dependent mechanism, then we would expect to see activation of caspase-3. At 4 d.p.f., activated caspase-3 labelling was only present in the *Tg(T α CP:EGFP)-pde6c*^{w59} mutant retina (compare Figures 3e and f), and at higher resolution, caspase-3 labelling was specifically in rod cells and no co-localization with GFP-expressing cones (Figure 3g). This suggested that caspase-dependent cell death was not contributing to cone photoreceptor cell death in the mutant retina, but rather to the dying rod photoreceptors.

As a number of different caspase-independent mechanisms of cell death have been reported in rodent models of retinal degeneration, we tested specific markers for these processes in the *pde6c*^{w59} zebrafish. In the *pde6c*^{w59} mutant retina, calpain activity was not detected in cone photoreceptors, although a low level of expression was observed in a few cells of the inner retina of both wild-type and mutant eyes at 4 d.p.f. (Figures 4a and d). Interestingly, the developing cornea in both wild-type and mutant eyes showed high levels of expression of calpain. Similarly, Parp staining was not present in the retina of either wild-type or mutant eyes (Figures 4b and e), neither was LC3 (mammalian homolog of Atg8 autophagy protein) staining²⁵ for autophagic vacuoles (data not shown). In contrast, high levels of rip1 staining co-localized with the dying GFP-expressing cone photoreceptor cells (Figure 4f). Confirmation of the immunohistochemical data was carried out by western blot analysis, which demonstrated that calpain levels were similar in both wild-type and mutant samples, whereas Parp levels were not detectable in either wild-type or mutant samples (Figure 4g). However, there was a sixfold increase in rip1 protein in the mutant eyes compared with wild-type levels (Figure 4g). These data suggested that the major cell death pathway activated in cone photoreceptors in the *pde6c*^{w59} mutant was necroptosis.

Rip3-dependent cone photoreceptor cell death. As RIP3 protein is the key activator of necroptosis, but available RIP3 antibodies do not recognize zebrafish rip3 protein, we took

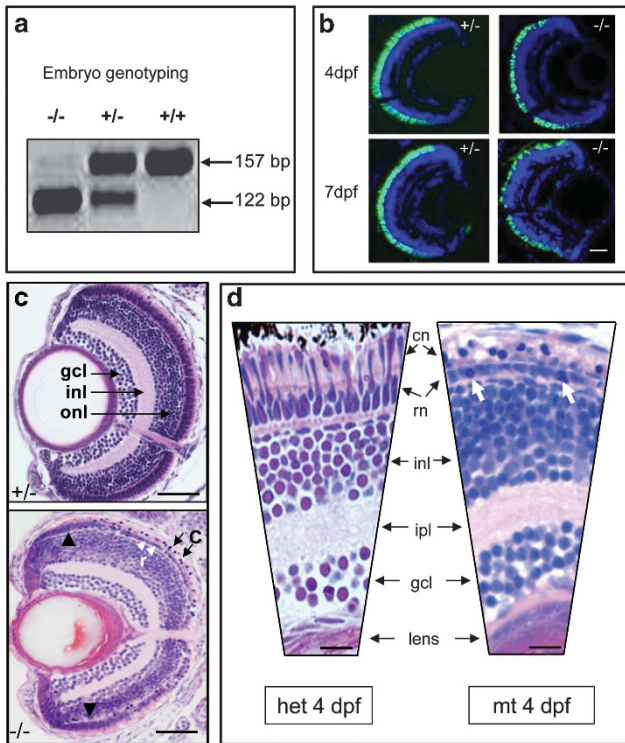


Figure 1 Genotyping and retinal histology for mutant *pde6c^{w59}* zebrafish. (a) Genotyping for mutation status using *Bsa*X1 restriction digest of *pde6c* PCR amplicon. Wild-type (+/+) band is 157 bp and the mutant (-/-) band is 122 bp. (b) Heterozygous (+/-) and mutant *pde6c* phenotype on transgenic background of GFP-expressing cone photoreceptors at 4 and 7 days post fertilization (d.p.f.) showing degeneration of cones. Scale bar = 20 μ m. (c) Comparison of sections through heterozygous (+/-) and mutant (-/-) retinas at 7 d.p.f. C, degenerating cones (black arrows); gcl, ganglion cell layer; inl, inner nuclear layer; onl, outer nuclear layer; r, single layer of rods (white arrowheads); black arrowheads, preserved peripheral retina. Scale bar = 50 μ m. Dorsal retina is at the top of each panel. (d) Higher magnification of heterozygous (het) versus mutant (mt) retina at 4 d.p.f. cn, cone nuclei; ipl, inner plexiform layer; rn, rod nuclei. Scale bar = 10 μ m. White arrows: condensed rod nuclei

advantage of fluorescent-activated cell sorting (FACS) from wild-type embryos on the Tg background and *Tg(T α CP:EGFP)-pde6c^{w59}* mutant embryos to isolate populations of GFP-positive cone cells (Figures 5a–d). From 300 embryos at 4 d.p.f. and 150 embryos at 7 d.p.f., we obtained approximately 70 000–100 000 EGFP-positive cells that were *zpr1* positive and isolated 250 ng of cone photoreceptor total RNA. Real-time reverse transcriptase-PCR (RT-PCR) analysis of *rip1* and *rip3* at 4 and 7 d.p.f. revealed that both genes were significantly upregulated in the mutant retina at both time points (Figure 5e, $P < 0.05$, $n = 9$).

As *rip3* expression was upregulated, we reasoned that morpholino knockdown of *rip3* in the mutant embryos could prevent necroptosis in the dying cones cells. Injection of either *rip3* antisense or mismatch morpholinos into wild-type embryos had no effect on wild-type *zpr1* cone-specific staining (Figures 6a and e). When mutant *pde6c^{w59}* embryos were injected with an antisense morpholino to *rip3*, we found that cone cell staining was similar to wild-type embryos when analyzed by *zpr1* immunohistochemistry (Figure 6b) compared with mismatch control injections, where a reduction in *zpr1* cone cell labelling was clearly evident (Figure 6f). TUNEL assays in *rip3* morphants demonstrated significantly fewer TUNEL-positive cells in the retina (Figure 6c) compared with the mismatch control injected embryos (Figure 6g; Supplementary Figure 1). Furthermore, when *rip3* RNA was co-injected with the *rip3* morpholino, it reversed the TUNEL staining levels (Figure 6d) to that seen in mismatch-treated *pde6c^{w59}* larvae (Figure 6g), showing specificity of the morpholino. As Rip3 can promote necroptosis through the production of ROS in the mitochondria,²⁶ we examined carbonyl adduct formation derived from protein oxidation in *pde6c^{w59}* mutant and *rip3* morphant *pde6c^{w59}* larvae. At both 4 and 7 d.p.f., the carbonyl content in *pde6c^{w59}* embryos was significantly increased ($P < 0.0001$; $n = 8$) compared with wild-type eyes (Figure 6h). However, in *rip3* morphants, the carbonyl content production was significantly reduced

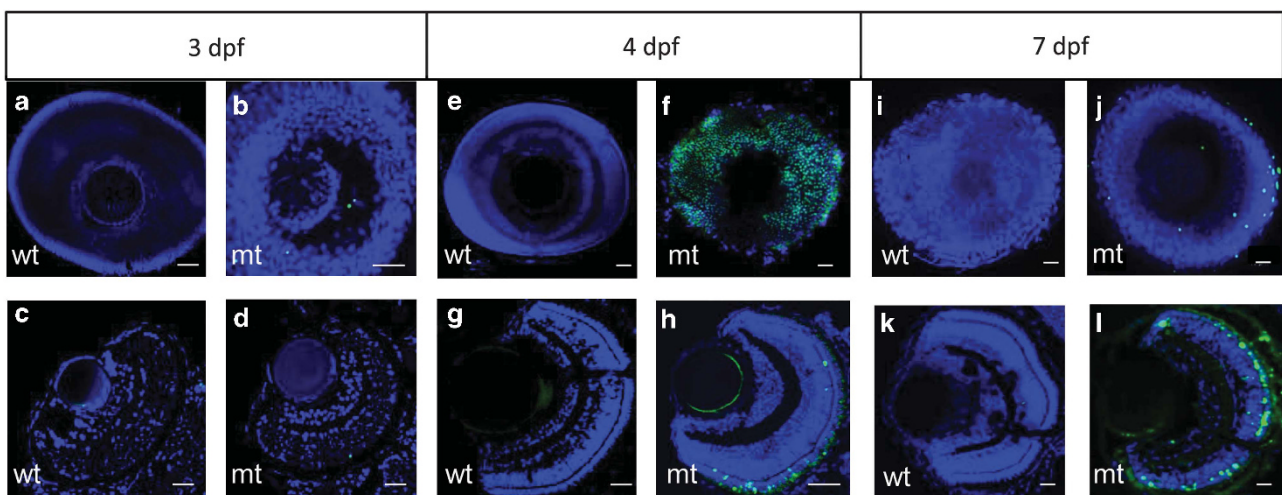


Figure 2 Time course of TUNEL staining in whole-mount and retinal sections. Representative images of whole-mount eyes and corresponding sections at the denoted ages of 3, 4 or 7 days post fertilization (d.p.f.). (a, b, e, f, i, k) Whole-mount eyes. (c, d, g, h, k, l) Retinal sections. mt, *pde6c^{w59}* mutant; wt, wild type. Scale bar is 20 μ m. TUNEL-positive cells, green labelling; 4',6-Diamidino-2-phenylindole counterstain for cell nuclei

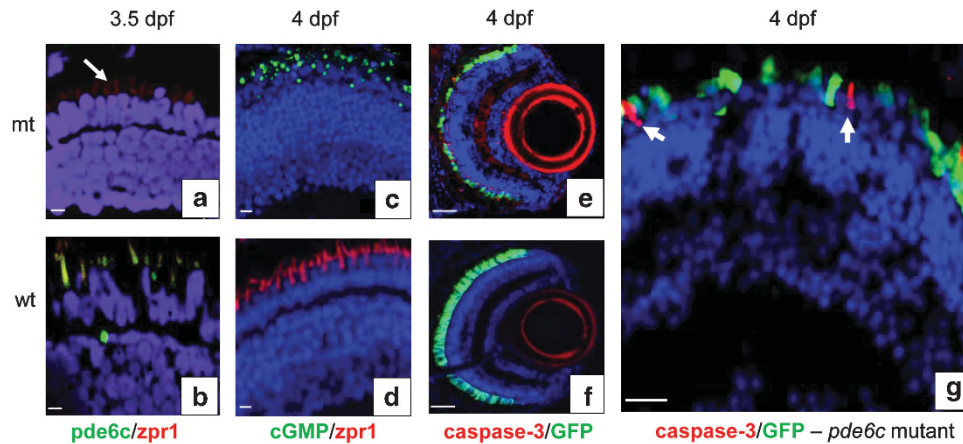


Figure 3 Expression of cell death markers in the retinal sections. (a, c, e, g) Mutant *pde6c* (mt) retinal images. (b, d, f) Wild-type (wt) retinal images. (a and b) Double immunostaining with *zpr1* cone-specific marker in red and *pde6c* in green. (c and d) Double immunostaining for cGMP labelling in green and *zpr1* in red. (e and f) Activated caspase-3 localization in red on GFP-expressing cone transgenic background. (g) Higher magnification of retina in image (e) showing no overlap of caspase-3 red staining in GFP-expressing cones (green). All sections counterstained with DAPI. Scale bar is 5 μm , except in e and f, where it is 20 μm

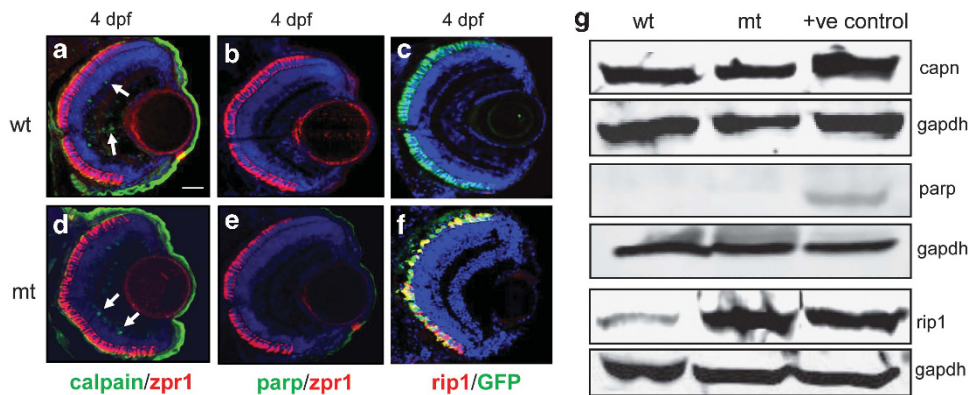


Figure 4 Expression patterns of caspase-independent cell death markers. (a–c) Wild-type (wt) retinal images. (d–f) Mutant *pde6c*^{-/-} (mt) retinal images. (a and d) Double labelling of calpain in green and *zpr1* cone-specific marker in red. A few cells express calpain in the inner retina (white arrows). Scale bar = 20 μm . (b and e) Double labelling of parp in green and *zpr1* in red. (c and f) *rip1* co-labelling in red on GFP-expressing cone transgenic background. (g) Western blot of calpain (capn), parp and *rip1* at 7 d.p.f. Positive (+ve) controls: for parp and capn, mouse E14.5 eye tissue; for *rip1*, HEK293 cell line. Gapdh used to normalize gel loading

compared with *pde6c*^{w59} mutant eyes ($P < 0.001$; $n = 8$). This demonstrates that activation of necroptosis leading to increased ROS production is *rip3*-dependent in the *pde6c*^{w59} mutant and that *rip3* deficiency suppresses ROS production and consequently oxidative damage to the retina.

As we found cone cell death to be mediated through the necroptosis pathway, we next asked what signalling mechanisms could lead to activation of necroptosis. cGMP-dependent protein kinase G (PKG) is one of the major cellular targets for cGMP in the retina,²⁷ therefore, we examined the expression of *pkg1* in mutant *pde6c*^{w59} retina and found this gene was upregulated from 3 d.p.f. (Supplementary Figure 2a). These results support a recent report showing that PKG was increased in a mouse model of retinal degeneration.²⁸ In addition, as Rip3 is known to be induced by tumor necrosis factor α (TNF α),²⁹ we examined the spatiotemporal expression pattern of TNF α in mutant *pde6c*^{w59} retina. TNF α expression began at 3 d.p.f. before cone cell death (Supplementary Figure 3) and was highly elevated at

4 d.p.f., co-incident with increased Rip1 upregulation (Supplementary Figure 3) and Rip3 upregulation (Supplementary Figure 2b).

To determine whether the retina was functionally responsive to light after *rip3* knockdown, we examined the visual background adaptation (VBA) response in morphant larvae. VBA is a neuroendocrine response used for camouflage where dark-adapted fish disperse their melanin granules (Figure 7a) and thus appear darker, whereas light-adapted fish aggregate their melanin into small granules (Figure 7b) and therefore appear more transparent.³⁰ As this response is driven through the retino-thalamic tract, blind fish are unable to exhibit this response (Figures 7e and f). After 30 min of dark adaptation followed by 15 min of bright light exposure, 7 d.p.f. wild-type larvae injected with either *rip3* morpholino or the mismatch control display small melanin granules as expected (Figures 7c and d). In contrast, *pde6c*^{w59} mutants injected with the mismatch control morpholino display larger diffuse melanin granules indicating visual impairment (Figure 7h).

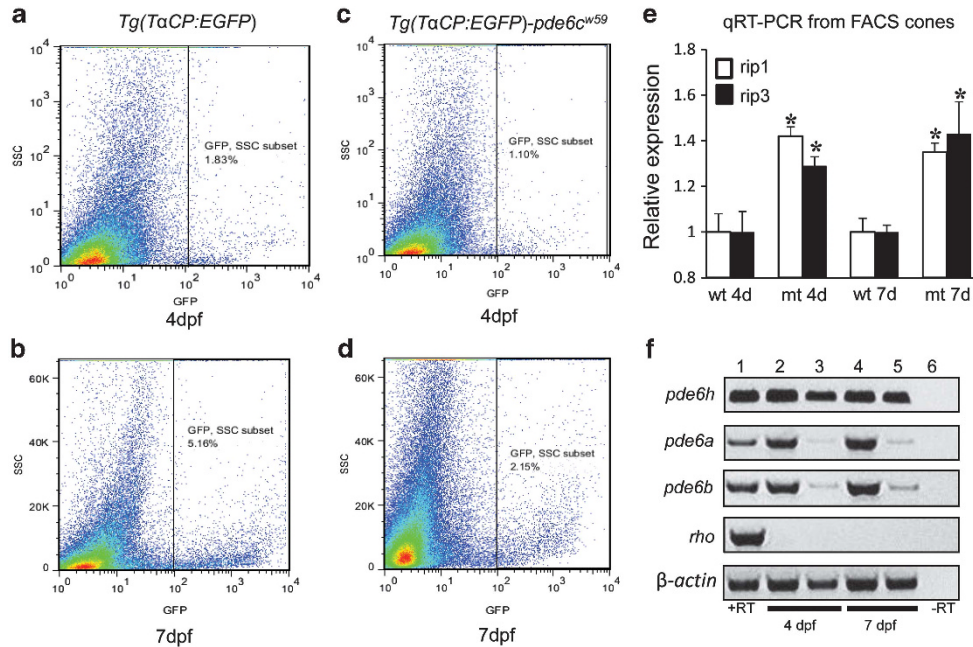


Figure 5 Flow cytometry sorting of fluorescent cone photoreceptors for gene expression analysis. (a and b) FACS plots for transgenic *Tg(TαCP:EGFP)* embryos that are wild type at the *pde6c*^{+/+} locus showing the side scatter (SSC) and EGFP profiles. (c and d) FACS plots for mutant *Tg(TαCP:EGFP)-pde6c*^{w59-/-} cone photoreceptors. (e) Quantification of real-time RT-PCR expression data for *rip1* and *rip3* from EGFP-positive cells at 4 and 7 d.p.f. in photoreceptors from wild-type (wt) and mutant (mt) embryos. Data presented as mean ± S.E.M. **P* < 0.05, *n* = 9. (f) Relative RT-PCR analysis for rod photoreceptor genes (*pde6a*, *pde6c*, *rho*), cone *pde6h* gamma subunit and *β-actin* internal control from whole adult retinal RNA (lanes 1 and 6); FACS-sorted mutant cone RNA (lanes 2 and 4); FACS-sorted wild-type cone RNA (lanes 3 and 5). RT, reverse transcriptase

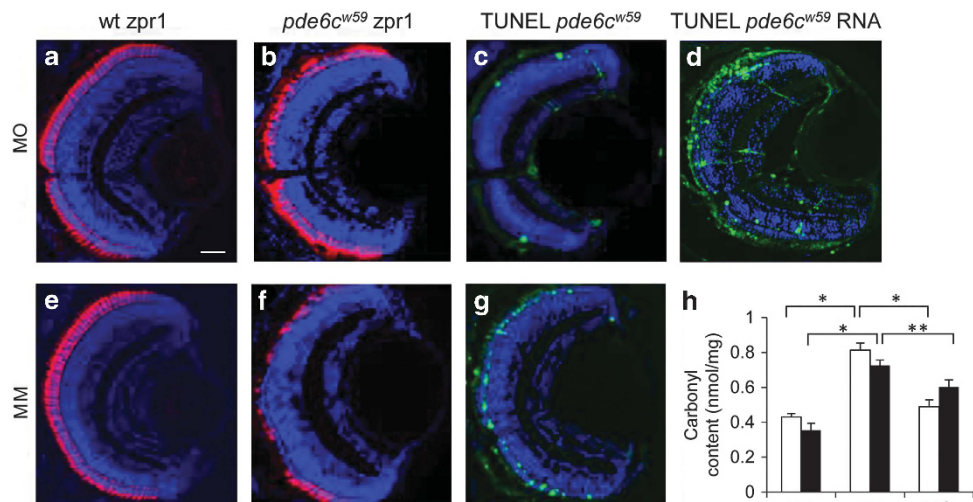


Figure 6 Phenotype at 4 d.p.f. after morpholino knockdown of *rip3* in wild-type (wt) and *pde6c*^{w59} mutant (mt) embryos. (a–d) *rip3* morpholino (MO) injection. (e–g) *rip3* mismatch morpholino (MM) injection. (a and e) Control injections of MO or MM in wt embryos. *Zpr1* cone-specific labelling in red. Scale bar = 20 μm. (b) *rip3* MO knockdown in mt embryos showing increased *zpr1* labelling in red. (c) TUNEL labelling in *rip3* MO knockdown mt embryos. (d) TUNEL labelling in mt embryos co-injected with *rip3* MO and *rip3* RNA. (f) *rip3* MM knockdown in mt embryos showing decreased *zpr1* labelling in red. (g) TUNEL labelling in mt embryos injected with *rip3* MM. (h) ELISA quantitation of carbonyl content in wt, mt and MO-injected embryos at 4 d.p.f. (white bars) or 7 d.p.f. (black bars). Mean ± S.E.M., *n* = 8, **P* < 0.0001; ***P* < 0.001

However, in *rip3* morphant *pde6c*^{w59} larvae, the melanin granules have reverted to the small wild-type appearance (Figure 7g), demonstrating that the VBA response is normalized. These data confirm that cone cell death in the *pde6c*^{w59} mutants is *rip3* dependent and that knockdown of *rip3* remarkably restores the responsiveness of the retina to light.

How this recovery of response to light occurs seems initially counterintuitive, as *rip3* knockdown would not replace the absence of *pde6c* α-subunit protein required for phototransduction. Furthermore, *pde6c*^{w59} mutants also display significant remodelling of second-order neurons (horizontal cells)³¹ that could limit communication with the inner retina

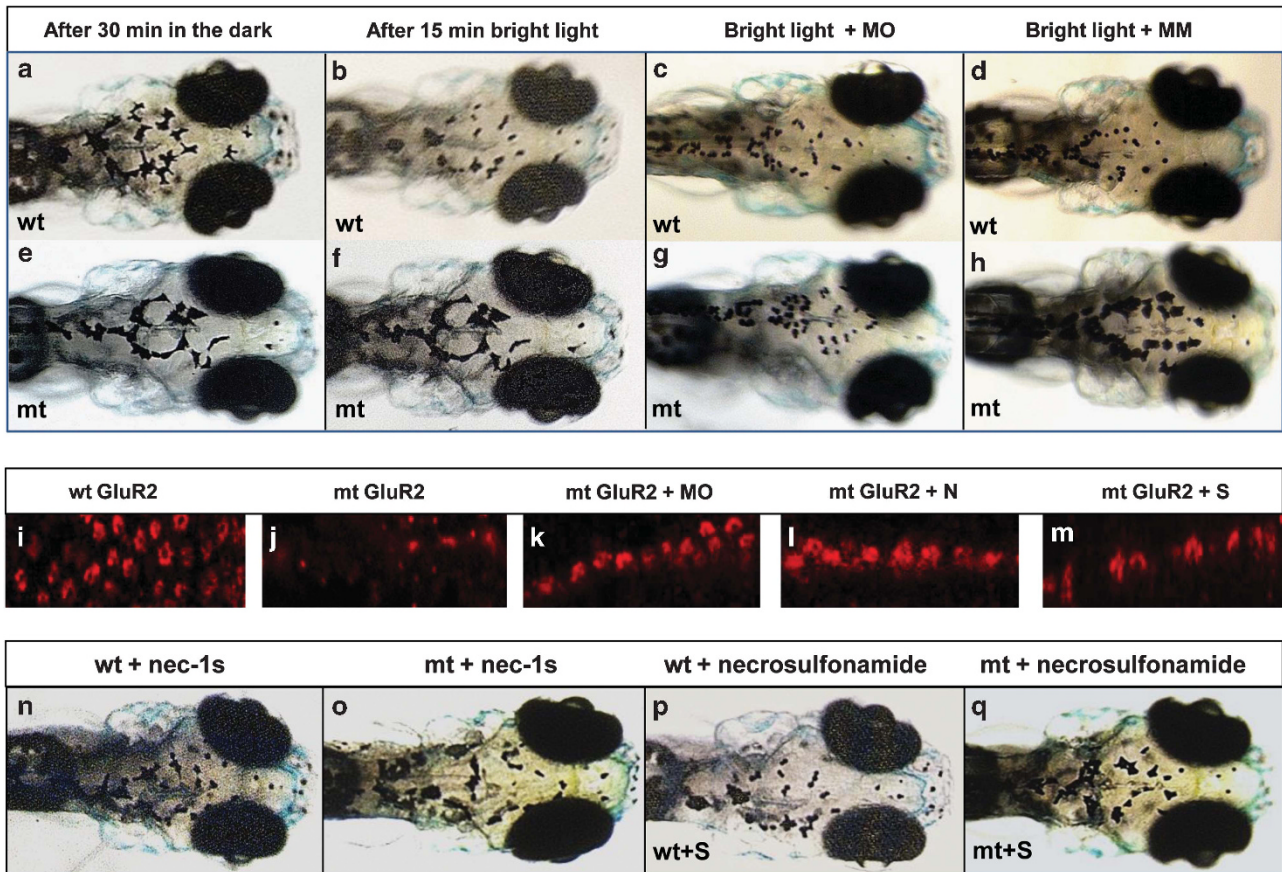


Figure 7 Visual background adaptation (VBA) in response to bright light stimulation at 7 d.p.f. Upper panels, wild-type (wt) embryos; lower panels, *pde6c*^{w59} mutant (mt) embryos. Representative images showing the distribution of melanin after dark adaptation (a and e); after light adaptation (b and f); after *rip3* morpholino (MO) injection (c and g); after mismatch control morpholino (MM) injection (d and h). (a and b) Images taken from the same wild-type larva before and after light adaptation. (e and f) Taken in the same mutant larva before and after light adaptation. (i) Labelling of GluR2 receptors in wt retina (i); mt retina (j); in *rip3* morphant retina (k); in retina treated with necrostatin-1s (l); in retina treated with necrosulfonamide (m). VBA response in wt (n) or mt larvae (o) treated with necrostatin-1s (N) showing small pigment granules. VBA response in wt (p) or mt larvae (q) treated with necrosulfonamide (S) showing small pigment granules

and thereby contribute to functional visual deficits. However, recently an elegant study in a mouse model lacking cone *Pde6c* showed that cones expressed the rod photoreceptor *Pde6a/b* subunit proteins and that these subunits were used instead for cone phototransduction.³² Therefore, the expression of rod phototransduction genes in FACS *Tg(TαC-P:EGFP)* wild-type and mutant cones was examined. We found that wild-type cones expressed very low levels of *pde6a* and *pde6b*, whereas mutant cones had highly upregulated levels of these two genes at both 4 and 7 d.p.f. (Figure 5f). Rhodopsin, which is a rod-specific gene, is not expressed in the FACS RNA samples, indicating that no contaminating rods were present. Presence of the cone-specific gamma subunit (*pde6h*) verified the presence of cone photoreceptor cells in all samples. Furthermore, we examined the expression of two photoreceptor-specific transcription factors *crx* and *nrl*, which are required to drive expression of *pde6a* and *pde6b*³³ and found they were expressed in mutant cone cells (Supplementary Figure 4). At 7 d.p.f. when *nrl* expression decreases in wild-type cones, it remains more highly expressed in mutant cones (Supplementary Figure 4). These results suggested that the VBA response observed in *rip3*

morphant *pde6c*^{w59} larvae most likely have occurred through upregulation of compensatory rod subunit proteins. To determine whether *rip3* knockdown was involved in remodelling of the inner retina, we examined immunolabelling for glutamate receptor subunit 2 (GluR2), which detects glutamate receptors on horizontal cell processes that synapse with rods and cones. In wild-type retina, GluR2-labelled horizontal cells synapsing with cone pedicles in a rosette-like cluster in the outer plexiform layer (Figure 7i), whereas in *pde6c*^{w59} mutant retina only punctate staining of rod spherules was apparent (Figure 7j). In *rip3* morphants, the GluR2 rosette staining pattern was present but there were fewer cones than in wild-type eyes (Figure 7k). In the presence of either necrostatin-1s (Figure 7l) or necrosulfonamide (Figure 7m), rosette staining for GluR2 was present, suggesting that second-order remodelling in the inner plexiform layer was a direct consequence of *rip3* signalling.

Pharmacological inhibition of cone and rod photoreceptor cell death. As RT-PCR revealed that both *rip1* and *rip3* were upregulated in *pde6c*^{w59} mutant cone photoreceptors, we took advantage of small-molecule drugs

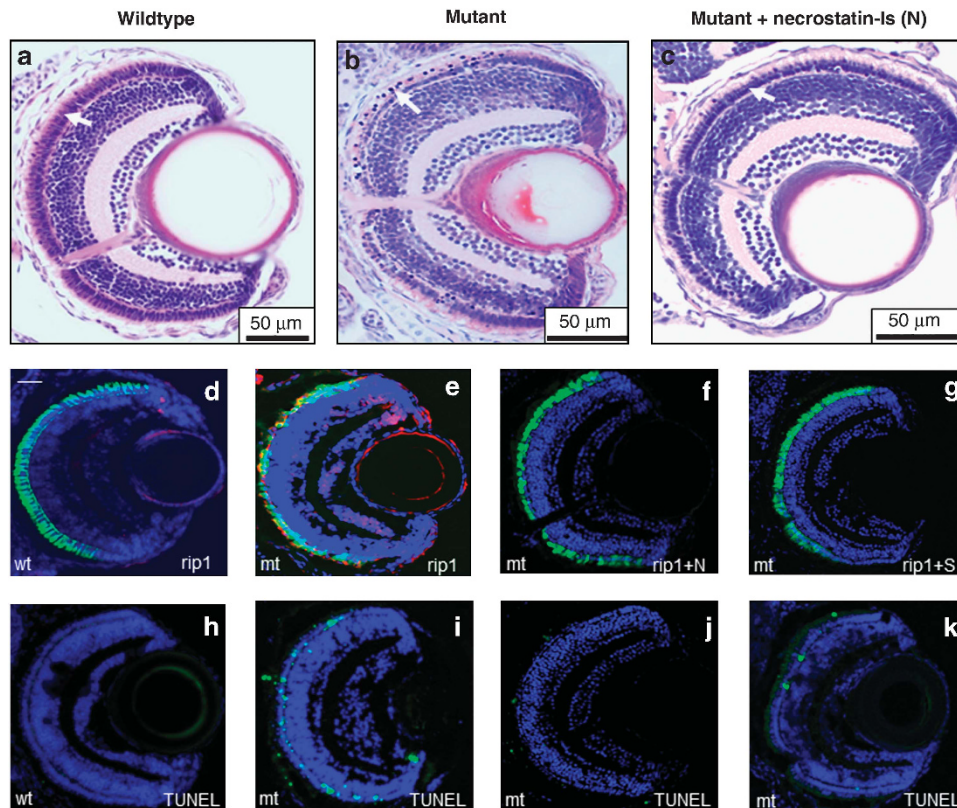


Figure 8 Effect of RIP signalling inhibitors on *pde6c*^{w59} mutant phenotype at 7 d.p.f. Retinal histology in (a) wild-type (wt), (b) untreated mutant (mt) and (c) mt retina from embryos treated with 100 mM necrostatin-1s (N). White arrows in a–c indicate the photoreceptor nuclear layer of the retina. Rip1 labelling (red) in wt retina (d), in mt retina co-localizing with EGFP-expressing cones that are dying (e), and in mt retina treated with necrostatin-1s (f). (g) rip1 labelling in the retina of *pde6c*^{w59} mutant embryos treated with 20 μM necrosulfonamide (S). TUNEL labelling in non-transgenic *pde6c*^{w59} mutant embryos (h–k) corresponding to the treatment panels (d–g) above. Scale bar in d = 20 μm

that target specifically RIP1³⁴ and RIP3 kinases³⁵ as potential pharmacological approaches to inhibit cone cell death. Using dose-response analysis in wild-type zebrafish,¹⁰ the highest concentration of necrostatin-1s (RIP1 inhibitor) and necrosulfonamide (RIP3 inhibitor) that could be utilized without causing toxicity to embryos was 100 and 20 μM, respectively. When *Tg(Tα:CP:EGFP)-pde6c*^{w59} mutant embryos were treated with 100 μM necrostatin-1s from 10 h.p.f. to 7 d.p.f., the outer retina was preserved resembling wild-type retina, with only occasional condensed nuclei present (Figures 8a–c). Rip1 labelling of cone cells in necrostatin-1s-treated mutants was not detected (Figure 8f) as in wild-type retina (Figure 8d), compared with untreated embryos where intense rip1 labelling co-localized with EGFP-expressing cone cells (Figure 8e). Only occasional TUNEL-positive cells were present in treated embryos (Figure 8j) compared with untreated mutants (Figure 8i). Rip1 labelling was also absent in embryos treated with 20 μM necrosulfonamide used to inhibit rip3 (Figure 8g) with a concomitant reduction in TUNEL staining (Figure 8k) compared with untreated embryos. These data establish that pharmacological targeting of Rip1 and Rip3 kinases inhibits cone photoreceptor cell death in the *pde6c*^{w59} zebrafish model. To test if the pharmacologically treated embryos were also responsive to light, VBA analysis revealed that in the presence of either necrostatin-1s (Figure 7o) or necrosulfonamide (Figure 7q)

melanin granule contraction was normalized compared with untreated larvae (Figure 7f).

Discussion

In this study, we report that cone-photoreceptor cell death in the retina of the blind *pde6c*^{w59} model of retinal degeneration occurs through a *rip3*-dependent pathway and that either genetic or pharmacological inhibition of necroptosis effectors rescues cone cell death and restores the responsiveness of the retina to light. In addition, we show that in genetically normal rod photoreceptors there is bystander cell death mediated through a caspase-dependent mechanism. Our data may provide an explanation of why using single inhibitors of cell death have had limited rescue effects and poor long-term outcomes when tested in other retinal degeneration models,^{36,37} because the rod and cone photoreceptors are dying by different mechanisms so eventually all the photoreceptors are lost. The significance of our findings is that combination therapy directed at the different cell death mechanisms would be crucial in designing effective treatment strategies.

A surprise finding in the study was that the visual response in *pde6c*^{w59} larvae was restored by *rip3* knockdown, despite the absence of a key phototransduction protein (*pde6c*). Recently, several studies have suggested that the linear rod

and cone phototransduction pathways can in fact couple to one another in disease states. For instance, in a genetically derived all-cone retina mouse model lacking cone Pde6c (*Nrl*^{-/-}; *cpfl1*), it was demonstrated that the cones instead expressed the rod Pde6 catalytic subunits conferring phototransduction capability to the cones.³² Similarly, in the *rd10* mouse (which lacks the rod *Pde6β* gene), the cone *Pde6α'* subunit was transgenically expressed in the mutant *rd10* rods and this rescued the response to light, demonstrating that cone *Pde6α'* can functionally substitute for *Pde6αβ*.³⁸ These studies suggest that the rod and cone Pde6 catalytic subunits can functionally substitute for one another and our work further implies that the local environment can determine rod and cone coupling. Although the exact mechanism by which *rip3* knockdown leads to upregulation of *pde6a* and *pde6b* remains to be determined, our data suggest that maintenance of high levels of the *nrl* transcription factor in cones is crucial to this process. We also found that the inner retina remodeling is inhibited when *rip3* is knocked down, which suggests that these secondary changes are directly related to cone cell death.

Although the exact mechanism by which activation of the RIP signalling pathway leads to cell death remains to be fully characterized, upregulation of RIP1 and RIP3 in cones cells provides evidence that the necroptosis pathway is the major cause of cone photoreceptor loss in *pde6c*-deficient zebrafish retina. Identification of the substrates for RIP1 and RIP3 kinases may lead to identification of further key effectors of necroptosis. Recent studies have revealed that increased RIP3 stimulates the production of ROS³⁹ because of increased oxidative phosphorylation and it is thought to result in a catastrophic overload to the metabolic state of the cell.²⁹ Our studies showing overproduction of ROS in the mutant *pde6c*^{w59} retina supports this downstream mechanism, suggesting that inhibition of oxidative stress may be a valid approach for inhibiting cone photoreceptor cell death in this model. Targeting the reduction of superoxide-free radicals using antioxidants such as *N*-acetylcysteine has been found to protect cone photoreceptors from bystander oxidative stress in mouse models of rod photoreceptor degeneration.⁴⁰

Further understanding of the detailed molecular mechanisms leading to necroptosis could reveal new targets that maybe developed as therapeutic interventions for many necroptosis-related diseases. Recently, four specific substrates for RIP3 have been identified (death-domain-associated protein 6 (Daxx), phosphoglycerate mutase family member 5 (PGAM5), DNA-dependent activator of IRF and sirtuin 2 (SIRT2)) as well as activation of a number of biochemical processes that are critical for necroptosis, which could each represent potential targets for inhibiting RIP3-dependent necroptosis in retinal degeneration. (i) RIP3-dependent phosphorylation of Daxx results in its nuclear export and subsequent retinal ganglion cell death upon a retinal ischemic injury insult.⁴¹ In RIP3-depleted cells, phosphorylation and nuclear export of Daxx is prevented thereby inhibiting retinal cell death. Thus, manipulating the nuclear trafficking of Daxx might be a possible option. (ii) The mitochondrial phosphatase PGAM5 was identified as a RIP3 substrate in HT-29 human cells,⁴² and these enzyme complexes with RIP1/RIP3/mixed lineage kinase-like in

necrosome. Inhibitors of PGAM5 might therefore prevent execution of necroptosis. (iii) DNA-dependent activator of IRF is thought to act as a DNA sensor that induces interferon-1 production and interacts with RIP3 during viral infection-induced necroptotic cell death,⁴³ so would most likely be beneficial for retinal degeneration associated with an immune response. (iv) Most recently, SIRT2 has been shown to regulate the deacetylation of RIP1, which is required for stable RIP1–RIP3 complex formation through RIP homotypic interaction motifs, and this deacetylation is RIP3-dependent process.⁴⁴ Using a small-molecule inhibitor of SIRT2 (known as AKG2), inhibition of dopaminergic neuronal cell death in a *Drosophila* model of Parkinson's disease has been demonstrated,⁴⁵ and could therefore be relevant for retinal degeneration.

Other biochemical activities that have been implicated in necroptotic cell death, including activation of phospholipase activity,⁴⁶ phosphorylation of signal transducer and activator of transcription 3⁴⁷ and mitochondrial membrane pore opening, regulated through cyclophilin D.⁴⁸ Very recently, involvement of cyclophilin D in necroptosis has been shown to be RIP3-dependent and that it can be inhibited by cyclosporin A.⁴⁹ This suggests that the neuroprotective effect provided by cyclosporin A that has been used previously to treat rats with diabetic retinopathy⁵⁰ and that can prevent the loss of the therapeutic cell transplants from dying in the retina⁵¹ could be in part the result of inhibiting RIP3-dependent necroptosis rather than due to its immunosuppressive activity alone.

A clearer picture is now emerging regarding photoreceptor cell death in retinal degenerative disorders. Rod cell death in animal models of retinitis pigmentosa was originally thought to be mainly caused by apoptotic mechanisms, however, there are now examples of activation of alternative cell death pathways contributing to the pathogenesis.³ Neuroprotection strategies targeting apoptotic rod cell death in animal models have proved effective,⁵² although such strategies have yet to be translated into effective clinical treatments.⁵³ This may be in part due to the observation that if the caspase-dependent cell death pathway is blocked then necroptosis is activated as a second line of defense.^{11,54} Less is known regarding cone cell death, however, loss of rod-derived growth factors, autophagy and oxidative stress are key contributors.^{4,55} As bystander defects are a major challenge for designing treatment strategies for retinal degeneration,²⁰ the different cell death mechanisms in the retina need to be identified, so that appropriate combinatorial strategies can be proposed. This is now possible based on a more sophisticated classification of cell death and an improvement in ways to detect the underlying cell signalling mechanisms.

The use of combination therapy in clinical ophthalmology is firmly established. For instance, treatment of recalcitrant glaucoma with combinations of drugs targeting different pathways provides synergistic effectiveness over individual treatment modalities.⁵⁶ We recently used a combinatorial approach of aminoglycoside read-through to treat the underlying genetic defect in the rat S334ter model coupled with glial-derived neurotrophic factor neuroprotection, which fully rescued the retinal degeneration, whereas individually we found that these treatments had limited efficacy.⁵⁷ In this study, we have shown that RIP3-dependent necroptosis is the

underlying molecular cause of cone cell death in the *pde6c*^{w59} model, whereas rod cells are dying via caspase-dependent apoptosis. Thus, development of effective treatment strategies for retinal degeneration affecting both rods and cones requires components that target both the primary genetic deficit and the secondary bystander cell loss.

Materials and Methods

Zebrafish maintenance and genotyping. Research was authorized by the University of British Columbia Animal Care Committee in accordance with the principles and guidelines of the Canadian Council of Animal Care and the Association for Research in Vision and Ophthalmology statement for the use of animals in vision research. Wild-type AB, *pde6c*^{w59} and *Tg[Tα:CP:GFP]²³* zebrafish strains were maintained as inbred stocks and staged according to morphological criteria. To visualize dying cone cells, we crossed the *pde6c*^{w59} mutation onto the *Tg[Tα:CP:GFP]* background where the cone α -transducin promoter drives GFP expression in all cone photoreceptors. Embryos were raised at 28.5 °C on a 14-h light/10-h dark cycle in 100 mm² Petri dishes containing standard embryonic medium 2 or embryonic medium 3 medium. High concentrations of paramnesia (3–10 × normal) were required to raise *pde6c*^{w59} mutant embryos to adulthood as the larvae do not normally survive past 10 d.p.f.. To aid image analysis where required, 0.2 mM phenylthiourea (Sigma-Aldrich, Oakville, ON, Canada) was added to the embryos at 10 h post fertilization (h.p.f.) to inhibit pigment formation. Genomic DNA was isolated from caudal fin tissue using a hot sodium hydroxide methodology.⁵⁸ After PCR amplification (*pde6c* primers: Forward: 5'-ttggcctcgaatactggctctc-3'; reverse: 5'-gttgaccagaacccggaag-3'), the 157 bp products were digested with *Bsa*X1 enzyme to determine genotype.

Histology, immunohistochemistry and TUNEL assay. Zebrafish embryos were fixed by immersion in 4% paraformaldehyde overnight at 4 °C. Fixed embryos were washed in phosphate-buffered saline (PBS) and then dehydrated through a graded ethanol series (50, 70, 90 and 100%), before being transferred to xylene and embedded in paraffin wax. Hematoxylin and eosin staining was carried out on 3–5 μ m thickness wax sections. For immunohistochemistry, embryos were infiltrated with 30% sucrose overnight at 4 °C before embedding in Polyfreeze medium (Polysciences, Warrington, PA, USA). Immunolabelling was carried out using 6- to 10- μ m thick frozen sections. The following primary antibodies were used: Pde6c polyclonal (1:50, Abcam, Eugene, OR, USA); Zpr-1 monoclonal (1:200, Zebrafish International Resource Center, Eugene, OR, USA). Zpr1 is a zebrafish cone-specific monoclonal antibody that was raised against zebrafish retinal extracts; cGMP polyclonal (1:200, Abcam); cleaved Parp polyclonal (1:200, Cell Signaling Technology, Danvers, MA, USA); calpain polyclonal (1:100, Novus Biologicals, Oakville, ON, Canada); cleaved caspase-3 monoclonal (1:200, Cell Signaling Technology); RIP1 polyclonal (1:100, Abcam); GluR2 monoclonal (1:75, Millipore, Billerica, MA, USA); Tnf- α polyclonal (1:30, Anaspec, Fremont, CA, USA). Secondary antibodies used were: Alexa Fluor 488 goat anti-rabbit immunoglobulin G or Alexa Fluor 546 goat anti-mouse immunoglobulin G (Life Technologies, Burlington, ON, Canada). For cGMP staining, the larvae were incubated in PBS with the phosphodiesterase inhibitor 3-isobutyl-1-methylxanthine (0.8 mM) for 10 min at 4 °C before fixation. Sections were incubated overnight at 4 °C with primary antibody diluted in blocking buffer. After extensive washes in PBS-Tween 20, localization of antibody labelling was detected by after 1 h incubation with secondary antibodies diluted in PBS containing 2% normal goat serum. Nuclei were counter stained with 4',6-diamidino-2-phenylindole and then images acquired using scanning laser microscopy. Transmitted light microscopy was used to capture images using a Zeiss Axioplan 2 microscope with D63ZNC DVC camera (Carl Zeiss, Toronto, ON, Canada). TUNEL staining in whole-mount eyes or retinal tissue sections was carried out as previously described.¹⁰ Images were acquired using a Zeiss 510 laser scanning confocal microscope (Carl Zeiss).

Immunoblotting. Briefly, 25 wild-type or mutant embryo eyes at 4 d.p.f. were snap frozen in liquid nitrogen and homogenized by sonication in lysis buffer (10 mM Tris pH 7.5, 10 mM NaCl, 1% SDS, 1 × Protease Inhibitor Cocktail (Roche, Mississauga, ON, Canada)). Insoluble material was removed by a 10-min centrifugation (25 000 × g). Protein concentration was determined by the DC protein assay (Bio-Rad, Hercules, CA, USA). Proteins (40 μ g) were separated on a 10% SDS-polyacrylamide gel, transferred to Immobilon-FL membrane

(Millipore), blocked in 5% non-fat milk powder in PBS/0.1% Tween-20 (PBST) for 2 h at RT and incubated overnight at 4 °C with primary antibody in the same buffer and diluted according to manufacturer's instructions. Following three washes in PBST, the membrane was incubated in the dark for 1 h with a Li-COR secondary antibody (IRDye 680LT goat anti-rabbit; Mandel Scientific, Guelph, ON, Canada), washed three times in PBST in the dark and protein bands were visualized using a Li-COR Odyssey detector (Mandel Scientific). NIH Image J software was used to quantify band intensities relative to glyceraldehyde-3-phosphate dehydrogenase (GAPDH) or β -actin loading controls (1:2000 GAPDH mouse monoclonal).

FACS for cones and qRT-PCR. To purify cone photoreceptors, we took advantage of FACS according to from previously published methods.⁵⁹ Briefly, 150–300 Tg *pde6c*^{+/+} and Tg *pde6c*^{w59/-} embryos were dechorionated, euthanized in tricaine and the eyes removed. Eyes were incubated in 1 × trypsin-EDTA solution for 7 min and then the reaction stopped by addition of 5% heat-inactivated FBS (Sigma-Aldrich). After centrifugation at 200 × g for 7 min, the pellet was incubated with FACSmax cell dissociation solution (AMS Biotechnology, Lake Forest, CA, USA) for 10 min at 37 °C and then a 1-ml syringe plunger was used to carefully dissociate the cells. Cells were filtered through a 40- μ m mesh cell strainer and then fluorescently sorted with a flow cytometer (BD Biosciences Influx Sorter; BD Biosciences, Mississauga, ON, Canada). RNA was isolated from the sorted cells using an RNeasy Micro kit (Qiagen, Mississauga, ON, Canada) and quantitated by NanoDrop spectrometry (Thermo Scientific, Wilmington, DE, USA). cDNA was amplified using QuantiTect Reverse Transcription Kit (Qiagen) and relative gene expression of *rip1* (NM_001043350), *rip3* (ENSDARG0000090965) and *gapdh* (NM_001115114) was quantified using the TaqMan primer and labelled probe protocol and the Viia 7 Real-Time PCR system (Applied Biosystems, Burlington, ON, Canada). Gene primers are listed in Supplementary Table 1. All reactions were performed using the TaqMan Universal Master Mix (2X), FAM-labelled TaqMan gene expression assays for *rip1* and *rip3*, VIC-labelled TaqMan endogenous control *gapdh* and 5 ng of cDNA. Thermocycling parameters were as follows: 2 min at 50 °C, 10 min at 95 °C, 40 cycles of 15 s at 95 °C, plus 60 s at 60 °C. Real-time PCR data were analyzed by the comparative C_T method. Each reaction was undertaken on three occasions, and for each of these, individual samples were subdivided into three aliquots for measurement.

Morpholino knockdown and RNA rescue. Morpholino sequence directed against the transcriptional start site of zebrafish *rip3* was designed by GeneTools: 5'-AGCGCATCTCTCCGCCGTCATCGC-3' (*rip3* MO) and mismatch (*rip3* MM) 5'-AGCCCCATGTCTCCCCCTCCATCCC-3' and were modified at the 3' end with carboxyfluorescein. Morpholinos were injected into the yolk of one or two cell stage wild-type or *pde6c* mutant embryos as follows: 2.5 ng each of *rip3* MO or *rip3* MM oligonucleotides (\pm 0.5 μ M morpholino to take into account off-target effects) were injected in 1 × Danieau buffer (58 mM NaCl, 0.7 mM KCl, 0.4 mM MgSO₄, 0.6 mM Ca (NO₃)₂, 5 mM HEPES, pH 7.6) with 0.1% phenol red using a Nanoject II variable injector (Drummond Scientific, Broomall, PA, USA). The morphant embryos were grown at 28.5 °C and observed for morphological changes under a stereoscopic microscope and fixed in 4% paraformaldehyde at 4 or 7 d.p.f. For RNA rescue experiments, 15 ng *rip3* RNA was co-injected with 2.5 ng *rip3* morpholino. Zebrafish *rip3* 5'-capped mRNA was synthesized as previously described,¹⁰ and primers for cloning the full-length cDNA is in Supplementary Table 1.

Detection of ROS. For each time point (4 or 7 d.p.f.), 150 eyes were obtained from wild-type, *pde6c*^{w59} mutant or *rip3*-knockdown *pde6c*^{w59} embryos. Protein extracts from eyes were isolated by adding 100 μ l of lysis buffer (50 mM Tris-HCl buffer pH 7.4, 0.1 mM EDTA, 0.1 mM ethylene glycol tetraacetic acid, 1 mM phenylmethyl sulfonyl fluoride, 2 μ M bestatin, 1 μ M pepstatin, 2 μ M leupeptin) and then sonicating samples for five cycles (30 s on–30 s off), followed by 5 × freeze-thawing. Lysates were centrifuged at 10 000 × g for 10 min at 4 °C and protein concentration in lysate supernatants was determined using the DC Protein assay (Bio-Rad). Quantitation of carbonyl adducts of proteins in 10 μ g eye extracts was determined using the OxiSelect Protein Carbonyl ELISA kit (Cell Biolabs, Inc., San Diego, CA, USA), according to manufacturer's instructions.

VBA assay. After morpholino injection, embryos were incubated at 28.5 °C for 7 d.p.f. Embryos were then transferred to a Petri dish and placed inside a box for dark-adaptation lasting 30 min. After placing the dish on the base of the microscope stand, a bright light was shined onto them from above. Images were

taken as soon as the light was switched on and again 15 min later to allow for full contraction of their melanophores as previously described.⁵⁰

Drug efficacy and treatment. After dechoriation of wild-type embryos at 10 h.p.f., a range of doses of necrostatin-1s (Biovision, Milpitas, CA, USA) or necrosulfonamide (Toronto Research Chemicals, Inc., Toronto, ON, Canada) were added directly to the aquarium water and then embryos were raised to 6 d.p.f. Each day the aquaria water containing drugs was refreshed. For each drug dose, 20 embryos were used in three independent experiments. The number of embryos surviving at 6 days was counted and quantitative data were expressed as mean \pm S.E.M. *Pde6c*^{w59} mutant embryos were treated with either 100 μ M necrostatin-1i or 20 μ M necrosulfonamide from 10 h.p.f. with assessment of the phenotypic effect at 7 d.p.f. by histology and immunocytochemistry.

Conflict of Interest

The authors declare no conflict of interest.

Acknowledgements. This work was supported by the Canadian Institutes of Health Research Team Grant (222728). We thank Dr. Susan Brockerhoff at University of Washington, USA, for kindly providing the *pde6c*^{w59} and *Tg[T α CP:GFP]* zebrafish lines and Dr. Anat Yanai for advice on FACS analysis.

- Chang GQ, Hao Y, Wong F. Apoptosis: final common pathway of photoreceptor cell death in rd, rds and rhodopsin mutant mice. *Neuron* 1993; **11**: 595–605.
- Marigo V. Programmed cell death in retinal degeneration: targeting apoptosis in photoreceptors as potential therapy for retinal degeneration. *Cell Cycle* 2007; **6**: 652–655.
- Sanch-Pelluz J, Arango-Gonzalez B, Kustermann S, Romero FJ, van Veen T, Zrenner E *et al*. Photoreceptor cell death mechanisms in inherited retinal degeneration. *Mol Neurobiol* 2008; **38**: 253–269.
- Paquet-Durand F, Silva J, Talukdar T, Johnson LE, Azadi S, van Veen T *et al*. Excessive activation of poly(ADP-ribose) polymerase contributes to inherited photoreceptor degeneration in the retinal degeneration mouse 1. *J Neurosci* 2007; **27**: 10311–10319.
- Kaur J, Mencl S, Sahaboglu A, Farinelli P, van Veen T, Zrenner E *et al*. Calpain and PARP activation during photoreceptor cell death in P23H and S334ter rhodopsin mutant rats. *PLoS One* 2011; **6**: e22181.
- Holler N, Zaru R, Micheau O, Thome M, Attinger A, Valitutti S *et al*. Fas triggers an alternative, caspase-8-independent cell death pathway using RIP as effector molecule. *Nat Immunol* 2000; **1**: 489–495.
- Hitomi J, Christofferson DE, Ng A, Yao J, Degterev A, Xavier RJ *et al*. Identification of a molecular signaling network that regulates a cellular necrotic cell death pathway. *Cell* 2008; **135**: 1311–1323.
- Trichonas G, Murakami Y, Thanos A, Morizane Y, Kayama M, Debouck CM *et al*. Receptor interacting protein kinases mediate retinal detachment-induced photoreceptor necrosis and compensate for inhibition of apoptosis. *Proc Natl Acad Sci USA* 2010; **107**: 21695–21700.
- Huang JF, Shang L, Zhang MQ, Wang H, Chen D, Tong JB *et al*. Differential neuronal expression of receptor interacting protein 3 in rat retina: involvement in ischemic stress response. *BMC Neurosci* 2013; **14**: 16.
- Viringipurampeer IA, Ferreira T, DeMaria S, Yoon JJ, Shan X, Moosajee M *et al*. Pax2 regulates a fadd-dependent molecular switch that drives tissue fusion during eye development. *Hum Mol Genet* 2012; **21**: 2357–2369.
- Degterev A, Hitomi J, Gemscheid M, Ch'en IL, Korkina O, Teng X *et al*. Identification of RIP1 kinase as a specific cellular target of necrostatins. *Nat Chem Biol* 2008; **4**: 313–321.
- He S, Wang L, Miao L, Wang T, Du F, Zhao L *et al*. Receptor interacting protein kinase-3 determines cellular necrotic response to TNF- α . *Cell* 2009; **137**: 1100–1111.
- Cho YS, Challa S, Moquin D, Genga R, Ray TD, Guildford M *et al*. Phosphorylation-driven assembly of the RIP1-RIP3 complex regulates programmed necrosis and virus-induced inflammation. *Cell* 2009; **137**: 1112–1123.
- Thiadens AA, Somervu V, van den Born LJ, van Schooneveld MJ, Kuijpers RW, van Moll-Ramirez N *et al*. Progressive loss of cones in achromatopsia: an imaging study using spectral-domain optical coherence tomography. *Invest Ophthalmol Vis Sci* 2010; **51**: 5952–5957.
- Pokorny J, Smith VC, Pinckers AJ, Cozijnsen M. Classification of complete and incomplete autosomal recessive achromatopsia. *Graefes Arch Clin Exp Ophthalmol* 1982; **219**: 121–130.
- Thiadens AA, Slingerland NW, Roosing S, van Schooneveld MJ, van Lith-Verhoeven JJ, van Moll-Ramirez N *et al*. Genetic etiology and clinical consequences of complete and incomplete achromatopsia. *Ophthalmology* 2009; **116**: 1984–1989.
- Thiadens AA, den Hollander AI, Roosing S, Nabuurs SB, Zekveld-Vroon RC, Collin RW *et al*. Homozygosity mapping reveals PDE6C mutations in patients with early-onset cone photoreceptor disorders. *Am J Hum Genet* 2009; **85**: 240–247.
- Kohl S, Coppieters F, Meire F, Schaich S, Roosing S, Brennenstuhl C *et al*. A nonsense mutation in PDE6H causes autosomal recessive incomplete achromatopsia. *Am J Hum Genet* 2012; **91**: 527–532.
- Stearns G, Evangelista M, Fadool JM, Brockerhoff SE. A mutation in the cone-specific *pde6* gene causes rapid cone photoreceptor degeneration in zebrafish. *J Neurosci* 2007; **27**: 13866–13874.
- Ripps H. Cell death in retinitis pigmentosa: gap junctions and the 'bystander' effect. *Exp Eye Res* 2002; **74**: 327–336.
- Evans K, Duval-Young J, Fitzke FW, Arden GB, Bhattacharya SS, Bird AC. Chromosome 19q cone-rod retinal dystrophy, Ocular phenotype. *Arch Ophthalmol* 1995; **113**: 195–201.
- Delyfer MN, Léveillard T, Mohand-Said S, Hicks D, Picaud S, Sahel JA. Inherited retinal degenerations: therapeutic prospects. *Biol Cell* 2004; **96**: 261–269.
- Kennedy BN, Alvarez Y, Brockerhoff SE, Stearns GW, Sappetto-Rebow B, Taylor MR *et al*. Identification of a zebrafish cone photoreceptor-specific promoter and genetic rescue of achromatopsia in the *nof* mutant. *Invest Ophthalmol Vis Sci* 2007; **48**: 522–529.
- Farber DB, Lolley RN. Cyclic guanosine monophosphate: elevation in degenerating photoreceptor cells of the C3H mouse retina. *Science* 1974; **186**: 449–451.
- Yokoyama T, Miyazawa K, Naito M, Toyotake J, Tauchi T, Itoh M *et al*. Vitamin K2 induces autophagy and apoptosis simultaneously in leukemia cells. *Autophagy* 2008; **4**: 629–640.
- Vanlangenakker N, Vandenberghe T, Bogaert P, Laukens B, Zobel K, Deshayes K *et al*. cIAP1 and TAK1 protect cells from TNF-induced necrosis by preventing RIP1/RIP3-dependent reactive oxygen species. *Cell Death Diff* 2011; **18**: 656–665.
- Paquet-Durand F, Hauck SM, van Veen T, Ueffing M, Ekström P. PKG activity causes photoreceptor cell death in two retinitis pigmentosa models. *J Neurochem* 2009; **108**: 796–810.
- Xu J, Morris L, Thapa A, Ma H, Michalakos S, Biel M *et al*. cGMP accumulation causes photoreceptor degeneration in CNG channel deficiency: evidence of cGMP cytotoxicity independently of enhanced CNG channel function. *J Neurosci* 2013; **33**: 14939–14948.
- Zhang DW, Shao J, Lin J, Zhang N, Lu BJ, Lin SC *et al*. RIP3, an energy metabolism regulator that switches TNF-induced cell death from apoptosis to necrosis. *Science* 2009; **325**: 332–336.
- Balm PH, Groneveld D. The melanin-concentrating hormone system in fish. *Ann NY Acad Sci* 1998; **839**: 205–209.
- Saade CJ, Alvarez-Delfin K, Fadool JM. Rod photoreceptors protect from cone degeneration-induced retinal remodeling and restore visual responses in zebrafish. *J Neurosci* 2013; **35**: 1804–1814.
- Kolandaivelu S, Chang B, Ramamurthy V. Rod phosphodiesterase-6 (PDE6) catalytic subunits restore cone function in a mouse model lacking cone PDE6 catalytic subunit. *J Biol Chem* 2011; **286**: 33252–33259.
- Nelson SM, Frey RA, Wardwell SL, Stenkamp DL. The developmental sequence of gene expression within the rod photoreceptor lineage in embryonic zebrafish. *Dev Dyn* 2008; **237**: 2903–2917.
- Takahashi N, Duprez L, Grootjans S, Cauwels A, Nerinckx W, DuHadaway JB *et al*. Necrostatin-1 analogues: critical issues on the specificity, activity and *in vivo* use in experimental disease models. *Cell Death Dis* 2012; **3**: e437.
- Sun L, Wang H, Wang Z, He S, Chen S, Liao D *et al*. Mixed lineage kinase domain-like protein mediates necrosis signalling downstream of RIP3 kinase. *Cell* 2012; **148**: 213–217.
- Drack AV, Dumitrescu AV, Bhattarai S, Gratie D, Stone EM, Mullins R *et al*. TUDCA slows retinal degeneration in two different mouse models of retinitis pigmentosa and prevents obesity in Bardet-Biedl syndrome type 1 mice. *Invest Ophthalmol Vis Sci* 2012; **53**: 100–106.
- Komeima K, Rogers BS, Campochiaro PA. Antioxidants slow photoreceptor cell death in mouse models of retinitis pigmentosa. *J Cell Physiol* 2007; **213**: 809–815.
- Deng W-T, Sakurai K, Kolandaivelu S, Kolesnikov AV, Dinculescu A, Li J *et al*. Cone phosphodiesterase-6 α restores rod function and confers distinct physiological properties in the rod phosphodiesterase-6 β -deficient rd10 mouse. *J Neurosci* 2013; **33**: 11745–11753.
- Goossens V, Grooten J, De Vos K, Fiers W. Direct evidence for tumor necrosis factor-induced mitochondrial reactive oxygen intermediates and their involvement in cytotoxicity. *Proc Natl Acad Sci USA* 1995; **92**: 8115–8119.
- Lee SY, Usui S, Zafar AB, Oveson BC, Jo YJ, Lu L *et al*. N-acetylcysteine promotes long-term survival of cones in a model of retinitis pigmentosa. *J Cell Physiol* 2011; **226**: 1843–1849.
- Lee YS, Dayma Y, Park MY, Kim KI, Yoo SE, Kim E. Daxx is a key downstream component of receptor interacting protein kinase 3 mediating retinal ischemic cell death. *FEBS Lett* 2013; **587**: 266–271.
- Wang Z, Jiang H, Chen S, Du F, Wang X. The mitochondrial phosphatase PGAM5 functions at the convergence points of multiple necrotic cell death pathways. *Cell* 2012; **148**: 228–243.
- Upton JW, Kaiser WJ, Mocarski ES. DAI/ZBP1/DLM-1 complexes with RIP3 to mediate virus-induced programmed necrosis that is targeted by murine cytomegalovirus vIRA. *Cell Host Microbe* 2012; **11**: 290–297.
- Narayan N, Lee IH, Borenstein R, Sun J, Wong R, Tong G *et al*. The NAD-dependent deacetylase SIRT2 is required for programmed necrosis. *Nature* 2012; **492**: 199–204.

45. Outeiro TF, Kontopoulos E, Altmann SM, Kufareva I, Strathearn KE, Amore AM *et al*. Sirtuin 2 inhibitors rescue α -synuclein-mediated toxicity in models of Parkinson's disease. *Science* 2007; **317**: 516–519.
46. De Valck D, Vercammen D, Fiers W, Beyaert R. Differential activation of phospholipases during necrosis or apoptosis: a comparative study using tumor necrosis factor and anti-Fas antibodies. *J Cell Biochem* 1998; **71**: 392–399.
47. Shulga N, Pastorino JG. GRIM-19 mediated translocation of STAT3 to mitochondria is necessary for TNF induced necroptosis. *J Cell Sci* 2012; **125**: 2995–3003.
48. Nakagawa T, Shimizu S, Watanabe T, Yamaguchi O, Otsu K, Yamagata H *et al*. Cyclophilin D-dependent mitochondrial permeability transition regulates some necrotic but not apoptotic cell death. *Nature* 2005; **434**: 652–658.
49. Tian W, Xu D, Han W, He H, Cai H, Chen H *et al*. Cyclophilin D modulates cell death transition from early apoptosis to programmed necrosis induced by honokiol. *Int J Oncol* 2013; **42**: 1654–1663.
50. Krügel K, Wurm A, Pannicke T, Hollborn M, Karl A, Wiedemann P *et al*. Involvement of oxidative stress and mitochondrial dysfunction in the osmotic swelling of retinal glial cells from diabetic rats. *Exp Eye Res* 2011; **92**: 87–93.
51. West EL, Pearson RA, Barker SE, Luhmann UF, Maclaren RE, Barber AC *et al*. Long-term survival of photoreceptors transplanted into the adult murine neural retina requires immune modulation. *Stem Cells* 2010; **28**: 1997–2007.
52. Bode C, Wolfgram U. Caspase-3 inhibitor reduces apoptotic photoreceptor cell death during inherited retinal degeneration in tubby mice. *Mol Vis* 2003; **9**: 144–150.
53. Talcott KE, Ratnam K, Sundquist SM, Lucero AS, Lujan BJ, Tao W *et al*. Longitudinal study of cone photoreceptors during retinal degeneration and in response to ciliary neurotrophic factor treatment. *Invest Ophthalmol Vis Sci* 2011; **52**: 2219–2226.
54. Vercammen D, Brouckaert G, Denecker G, Van de Craen M, Declercq W, Fiers W *et al*. Dual signaling of the Fas receptor: initiation of both apoptotic and necrotic cell death pathways. *J Exp Med* 1998; **188**: 919–930.
55. Léveillard T, Mohand-Saïd S, Lorentz O, Hicks D, Fintz AC, Clérin E *et al*. Identification and characterization of rod-derived cone viability factor. *Nat Genet* 2004; **36**: 755–759.
56. Gheith ME, Mayer JR, Siam GA, Monteiro de Barros DS, Thomas TL, Katz LJ. Managing refractory glaucoma with a fixed combination of bimatoprost (0.03%) and timolol (0.5%). *Clin Ophthalmol* 2008; **2**: 15–20.
57. Gregory-Evans K, Po K, Francis Chang F, Gregory-Evans CY. Pharmacological enhancement of *ex vivo* gene therapy neuroprotection in a rodent model of retinal degeneration. *Ophthalmol Genet* 2012; **47**: 32–38.
58. Meecker ND, Hutchinson SA, Ho L, Trede NS. Method for isolation of PCR-ready genomic DNA from zebrafish tissues. *Biotechniques* 2007; **43**: 610–614.
59. Manoli M, Driever W. Fluorescence-activated cell sorting (FACS) of fluorescently tagged cells from zebrafish larvae for RNA isolation. *Cold Spring Harb Protoc* 2012; e-pub ahead of print 1 August 2012; doi:10.1101/pdb.prot069633.
60. Fleisch VC, Neuhauss SC. Visual behavior in zebrafish. *Zebrafish* 2006; **3**: 191–201.

Supplementary Information accompanies this paper on Cell Death and Differentiation website (<http://www.nature.com/cdd>)